A new triple correlation technique for measuring ultrashort laser pulses

Nicholas G. Paulter, Jr.
National Institute of Standards and Technology, Electromagnetic Fields Division, Boulder, Colorado

Arun K. Majumdar[a)]
Department of Electrical Engineering, University of Colorado, Denver, Colorado

(Received 8 June 1990; accepted for publication 12 November 1990)

A new triple correlation technique for measuring the complete intensity profile of ultrashort optical pulses is described. The triple correlation preserves the phase information of the input pulse so that a reconstruction of the triply correlated signal will provide a unique reconstruction of the input. The new technique described here uses two second-order, nonlinear optical interactions for the generation of a triply correlated signal. A derivation of the measured triple-correlation signal and the pulse reconstruction is given. The effects of noise on the measured signal are also examined.

I. INTRODUCTION

The rapid progress of short-pulse laser technology has produced a concomitant increase in the use of ultrashort laser pulses for measuring various transient phenomena (see Refs. 1–6 for examples). The advantage of using ultrashort optical pulses for studying transient phenomena is the high temporal resolution offered by measurement techniques that use these pulses. These measurement techniques are pump-probe techniques, where one optical pulse is used to pump, or create, an event and another optical pulse is used to probe, or interrogate, that event or some manifestation of that event. Moreover, because the pump and probe pulses may be derived from a single pulse, measurement jitter can be eliminated. As the time duration of the phenomenon under investigation approaches the optical pulse widths that are used to measure them, it becomes essential that the temporal pulse profile be accurately known in order to correctly describe the phenomenon.

Currently available electronic test equipment do not have the temporal resolution necessary to measure the profile of ultrashort optical pulses. The fast response times and low jitter needed to measure these pulses are provided by only a few techniques. Other than the streak camera (the fastest measured response time being about 1 ps[7]) all these techniques use self-measurement schemes that exploit the extremely fast nonlinear optical response times found in some dielectric materials. These nonlinear optical techniques are based on the correlation of multiple replicas of the input pulse via second- or third-order nonlinear optical interactions in a material.

Degenerate four-wave mixing (DFWM), a third-order nonlinear optical technique, uses the correlation of three replicas of the input pulse to profile the input pulse[8–12] without loss of phase information. The drawback with DFWM is the use of the third-order nonlinear susceptibilities, which are often so small as to require pump intensities that approach, or exceed, the damage threshold of the material.[13,14] The commonly used intensity autocorrelation[15–18] uses two replicas of the input pulse and does not preserve the phase information of the pulse, so that any asymmetries will not be recovered from the measured signal. Interferometric autocorrelation[19] techniques require additional measurements (and equipment) to completely describe an optical pulse, thereby increasing the cost and complexity of analysis. Other double-correlation techniques[20,21] require nonlinear processes to modify the pulse in one (or both) of the arms of an autocorrelator. Unless these processes are well characterized it will be impossible to accurately reconstruct the input pulse.

A new triple-correlation method for measuring the complete temporal intensity profile of ultrashort laser pulses is proposed. Gamo first suggested triple correlation techniques for measuring optical pulses in 1963 when he proposed electronically mixing the outputs of three detectors that had each received a time-delayed portion of the input pulse.[22] With the ultrashort optical pulses used today, this technique would not be practical, though it does present the idea which is used in this study. In 1983, Wirnitzer proposed a triple correlator[23] based on the same design as Gamo's but using nonlinear optics to mix the three beams. The problem inherent in this technique is the high input powers required in order to observe the third-order effect.

II. PROPOSED TRIPLE CORRELATION USING NONLINEAR OPTICAL METHODS

The triple correlation technique proposed here for the measurement of ultrashort optical pulses uses two consecutive second-order nonlinear interactions of replicas of these pulses in a dielectric crystal. Because this technique is a triple correlation, it requires the interaction of three replicas of the optical pulse. The first nonlinear interaction, between two of the replicas, generates a second harmonic signal. The next interaction involves this second harmonic and the third replica. The output of this interaction may be either at the sum or difference frequency of the two inputs. As compared to Wirnitzer's proposed triple correlator, this proposed technique takes into consideration the need to

[a)]Also a Visiting Professor at NIST, Boulder, CO.

eliminate unwanted background signals and to optimize phase matching, and the limitations of the nonlinear properties of real materials. This triple correlation technique offers advantages over the previously discussed techniques for the measurement of ultrashort optical pulses because it will not require additional techniques (such as pulse amplification, compression, etc.) to profile the pulses.

The process of measuring ultrashort optical pulses using this triple-correlation technique is to first (a) obtain the two dimensional data corresponding to the triply correlated signal; (b) perform a two-dimensional Fourier transform on this data to obtain a bispectrum; (c) reduce the bispectrum to normal spectrum; and finally (d) inverse Fourier transform the spectrum to obtain the reconstructed profile of the ultrashort optical pulse. In Sec. II A, we derive an expression describing the triply correlated signal; in Sec. II B we present the two-dimensional Fourier transform and develop the bispectrum reduction technique. Simulations of the triple correlation and the effects of noise on the reconstructed signal are presented in Sec. III.

A. Derivation of triple-correlation signal

The triply correlated signal intensity will be derived here. Let the fields of the three interacting optical waves be (see Fig. 1)

$$E(t)=A(t)\cos[wt+\Phi(t)], \tag{1a}$$

$$E(t+\tau_1)=B(t+\tau_1)\cos[wt+w\tau_1+\Phi(t+\tau_1)], \tag{1b}$$

$$E(t+\tau_2)=C(t+\tau_2)\cos[wt+w\tau_2+\Phi(t+\tau_2)], \tag{1c}$$

where τ_1 and τ_2 are the time delays between the pulses. Let the interaction constants for the first nonlinear interaction be d_1 and for the second interaction be d_2, where these

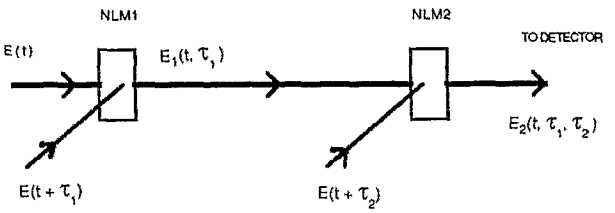

FIG. 1. Simple geometry for generating a triply correlated pulse by using two nonlinear interactions. $E(t)$, $E(t+\tau_1)$, and $E(t+\tau_2)$ represents the optical fields of the three laser pulse replicas, where τ_1 and τ_2 are delays. $E_1(t,\tau_1)$ is generated by the interaction of $E(t)$ with $E(t+\tau_1)$ in nonlinear medium, NLM1. The triply correlated field, $E_2(t,\tau_1,\tau_2)$, is created by the interaction of $E_1(t,\tau_1)$ and $E(t+\tau_2)$ in NLM2.

constants include geometrical factors as well as the nonlinear optical coefficients. Also, for simplicity, let the argument of the cosine functions in (1) be a, b, and c for $E(t)$, $E(t+\tau_1)$, and $E(t+\tau_2)$, respectively. Considering the interaction in the first crystal, between $E(t)$ and $E(t+\tau_1)$, the optical field generated is

$$\begin{aligned}E'_1(t,\tau_1)&=d_1[E^2(t)+E^2(t+\tau_1)+\mathrm{E}(t)E(t+\tau_1)]\\&=d_1[A^2(t)\cos^2(a)+B^2(t+\tau_1)\cos^2(b)\\&\quad+A(t)B(t+\tau_1)\cos(a)\cos(b)].\end{aligned} \tag{2}$$

If the optics are arranged so that the self-second-harmonic generated pulses do not contribute to the measured signal, we get

$$E_1(t,\tau_1)=d_1[A(t)B(t+\tau_1)\cos(a)\cos(b)].$$

Now we let E_1 interact with the pulse of the last beam, $E(t+\tau_2)$. Assuming the optics are arranged so that we do not detect the self-second-harmonic pulses, we get

$$\begin{aligned}E_2(t,\tau_1,\tau_2)&=d_1d_2E_1(t,\tau_1)E(t+\tau_2)=(d_1d_2)A(t)B(t+\tau_1)C(t+\tau_2)\cos(a)\cos(b)\cos(c)\\&=[(d_1d_2)/4]A(t)B(t+\tau_1)C(t+\tau_2)[\cos(a+b+c)+\cos(a+b-c)\\&\quad+\cos(a-b+c)+\cos(a-b-c)].\end{aligned} \tag{3}$$

The quantity measured by the detector is the integral of the intensity of the pulse described by E_2, and is given by

$$I_t(\tau_1,\tau_2)=1/\delta\int_{-\infty}^{\infty}E_2^2(t,\tau_1,\tau_2)dt, \tag{4}$$

where δ is the wave impedance of the nonlinear material. Putting (3) in (4) and noting that the time average of the squares of the cross products of the cosine terms will be zero and the time average of the squared like-terms (four of them) will be 2, we get

$$I_t(\tau_1,\tau_2)=\frac{4(d_1d_2/4)^2}{\delta}\int_{-\infty}^{\infty}A^2(t)B^2(t+\tau_1)C^2(t+\tau_2)dt=\frac{(d_1d_2)^2}{4\delta}\int_{-\infty}^{\infty}A^2(t)B^2(t+\tau_1)C^2(t+\tau_2)dt. \tag{5}$$

It is important to note that I_t is a function of two delays, τ_1 and τ_2. Next, the signal recovery procedure is discussed.

B. Signal recovery

Equation (5) needs to be rewritten for frequency domain analysis,

$$I(f_1,f_2)=\int_{-\infty}^{\infty}\int_{-\infty}^{\infty} I_t(\tau_1,\tau_2)\exp[-i2\pi(\tau_1 f_1+\tau_2 f_2)]d\tau_1\tau_2$$

$$=\frac{(d_1d_2)^2}{4\delta}\int_{-\infty}^{\infty}\int_{-\infty}^{\infty}\int_{-\infty}^{\infty}\{A^2(t)B^2(t+\tau_1)C^2(t+\tau_2)\exp[-i2\pi(\tau_1 f_1+\tau_2 f_2)]\}dt\,d\tau_1 d\tau_2. \quad (6)$$

Performing the integrations, we can obtain,

$$I(f_1,f_2)=[(d_1d_2)^2/4\delta]I(f_1)I(f_2)I(-f_1-f_2). \quad (7)$$

This result is the bispectrum. The discrete analog of (7) would be obtained after acquiring the two-dimensional (2-D) data and performing a discrete Fourier transform. Examination of the discrete bispectrum reveals

$$I_{i,j}=[(d_1d_2)^2/4\delta]I_iI_jI_{-i-j}, \quad (8)$$

where the i and j subscripts denote specific frequencies. The next step is then to convert the discrete bispectrum given by (8) into a (regular) discrete spectrum. Before doing this we can simplify the conversion by making use of symmetry relationships[24] and the fact that $I(\tau_1,\tau_2)$ is real (that is, zero imaginary parts). These symmetry relationships are shown graphically in Fig. 2. Because $I(\tau_1,\tau_2)$ is real, $I(f_1,f_2)$ is Hermitian, and consequently $I(f_1,f_2)=I^*(-f_1,-f_2)$. This reduces the problem of analyzing the entire bispectrum to analyzing only two quadrants. We can simplify even further. From (7) and ignoring the constants, we see

$$I(f_1,f_2)=I(f_1)I(f_2)I(-f_1-f_2)$$
$$=I(f_2)I(f_1)I(-f_2-f_1)$$
$$=I(f_2,f_1). \quad (9)$$

Similar symmetry relationships can be found for $I(f_1,-f_1-f_2)$ and $I(-f_1-f_2,f_2)$,

$$I(f_1,-f_1-f_2)=I(f_1)I(-f_1-f_2)I[-(-f_1-f_2)-f_1]$$
$$=I(-f_1-f_2)I(f_1)I(f_2)$$
$$=I(-f_1-f_2,f_2). \quad (10)$$

The symmetry and Hermiticity of $I(f_1,f_2)$ shows that there is only one unique octant in the bispectrum. This octant in turn can be used to produce a unique spectrum corresponding to the original triple-correlator input pulse. The inverse fourier transform of this spectrum provides our time domain waveform, which is a unique temporal profile of the input ultrashort optical pulse.

To reconstruct the spectrum from the bispectrum, first reexamine (8),

$$I_{i,j}=DI_iI_jI^*_{(i+j)}, \quad (11)$$

where the conjugate has been used in place of the negative frequencies and D represents all constants. In the octant of the bispectrum that will be used to obtain the spectrum, both i and j are non-negative and $i+j$ must be less than or equal to the maximum value of either i or j, which is N. Thus, the usable part of the unique octant is reduced by half and the equation needed to obtain the spectrum is,

$$I_{(i+j)}=[(I_{i,j})/I_iI_j]^*, i+j\leqslant N;\ 0\leqslant i,j\leqslant N. \quad (12)$$

The zeroth harmonic and next two harmonics for the spectrum will now be calculated. These are given by

$$I_0=(I_{0,0})^{1/3}, \quad (13a)$$

$$I_1=[(I_{1,0})/I_0]^{1/2}, \quad (13b)$$

$$I_2=[(I_{1,1})/(I_1I_1)]^*. \quad (13c)$$

Because the zeroth $(i,j=0)$ component of the bispectrum is real, so will be the zeroth $(i+j=0)$ component of the spectrum. The first harmonic $(i+j=1)$, however, is also

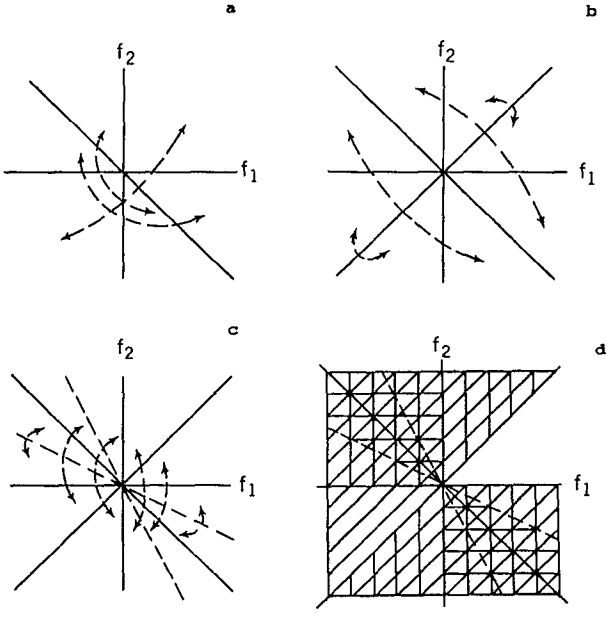

FIG. 2. Symmetry relations of bispectrum. Different areas of the bispectrum contain redundant information, and this fact is more easily seen by separating out the bispectrum symmetry relationships that give rise to the redundancy. These symmetries are caused by (a) hermiticity of the data, (b) $I(1,2)=I(2,1)$, and (c) $I(1,-1-2)=I(-1-2,2)$. The shaded areas in (d) exhibit the redundancy of bispectrum, showing that only one unique octant exists.

real. Therefore it appears we have lost the phase information for the first harmonic of the spectrum; this point will be dealt with in more detail later. The apparent loss of the first harmonic phase component is a linear phase error, and is more clearly seen from the following representation of (12) to compute the harmonics I_2, I_3, and I_4:

$$I_2 = M_2 \exp i\Phi_2$$
$$= [(M_{1,1})/(M_1 M_1)] \exp i(2\Phi_1 - \Phi_{1,1}), \quad (14a)$$

$$I_3 = M_3 \exp i\Phi_3$$
$$= [(M_{1,2})/(M_1 M_2)] \exp i(\Phi_1 + \Phi_2 - \Phi_{1,2})$$
$$= [(M_{1,2})/(M_1 M_2)] \exp i(3\Phi_1 - \Phi_{1,2} - \Phi_{1,1}), \quad (14b)$$

$$I_4 = M_4 \exp \Phi_4$$
$$= [(M_{2,2})/(M_2 M_2)] \exp i(2\Phi_2 - \Phi_{2,2})$$
$$= [(M_{2,2})/(M_2 M_2)] \exp i(4\Phi_1 - 2\Phi_{1,1} - \Phi_{2,2}), \quad (14c)$$

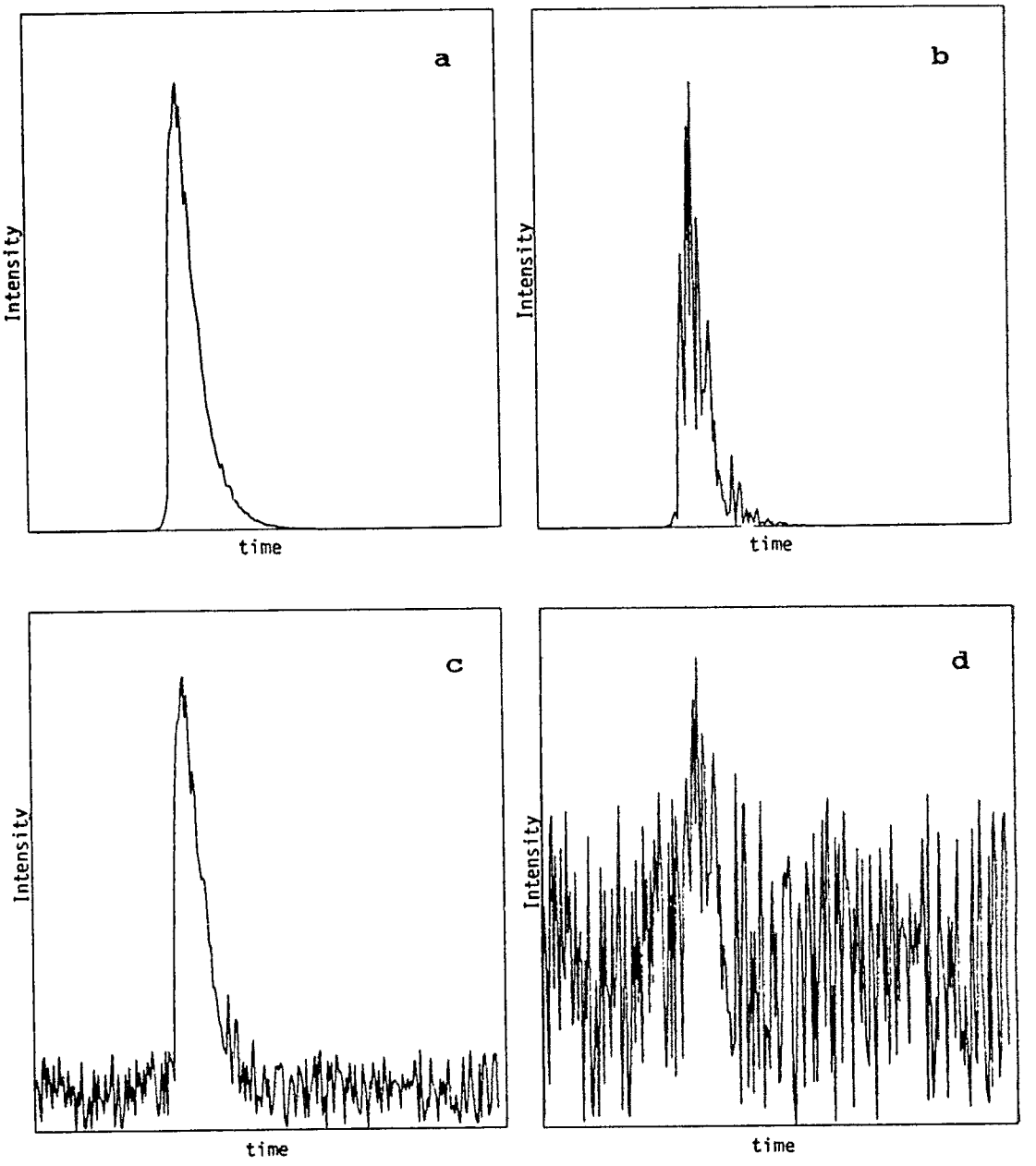

FIG. 3. Test waveforms with noise. (a) and (b) show the test waveform (double-sided exponential) with multiplicative noise and (c) and (d) show the test waveform with additive noise. The peak signal-to-noise ratio in (a) and (c) is 5, and in (b) and (d) is 0.5.

and

$$I_4=[(M_{1,3})/(M_1M_3)]\exp i(\Phi_1+\Phi_3-\Phi_{1,3})$$
$$=[(M_{1,3})/(M_1M_3)]\exp i(4\Phi_1-\Phi_{1,1}-\Phi_{1,2}-\Phi_{1,3}), \quad (15)$$

where M indicates the magnitude of the frequency component and Φ the phase.

One last point regarding the extraction of the spectrum from the bispectrum. This process can be performed in two different ways; one way averages the bispectrum and the other does not. To clarify this, consider the previous example for obtaining the fourth harmonic. In the nonaveraging technique, I_4 is obtained directly from either (14c) or (15). For the general case of using the nonaveraging technique (set $j=2$), the spectrum is given by

$$I_{i+2}=[(I_{i,2})/(I_iI_2)]^*, \quad i=1,2,...,N-2. \quad (16)$$

In the averaging technique, I_4 is obtained from the average of (14c) and (15). The spectrum, for the general case of using the averaging technique, is given by

$$I_{i+j}=(1/k)\Sigma[(I_{i,j})/(I_iI_j)]^*, \; i+j=3,4,...,N; i,j\geqslant 1, \quad (17)$$

where k is the integer value of $(i+j)/2$. And, as mentioned before, we need only consider one octant, so that

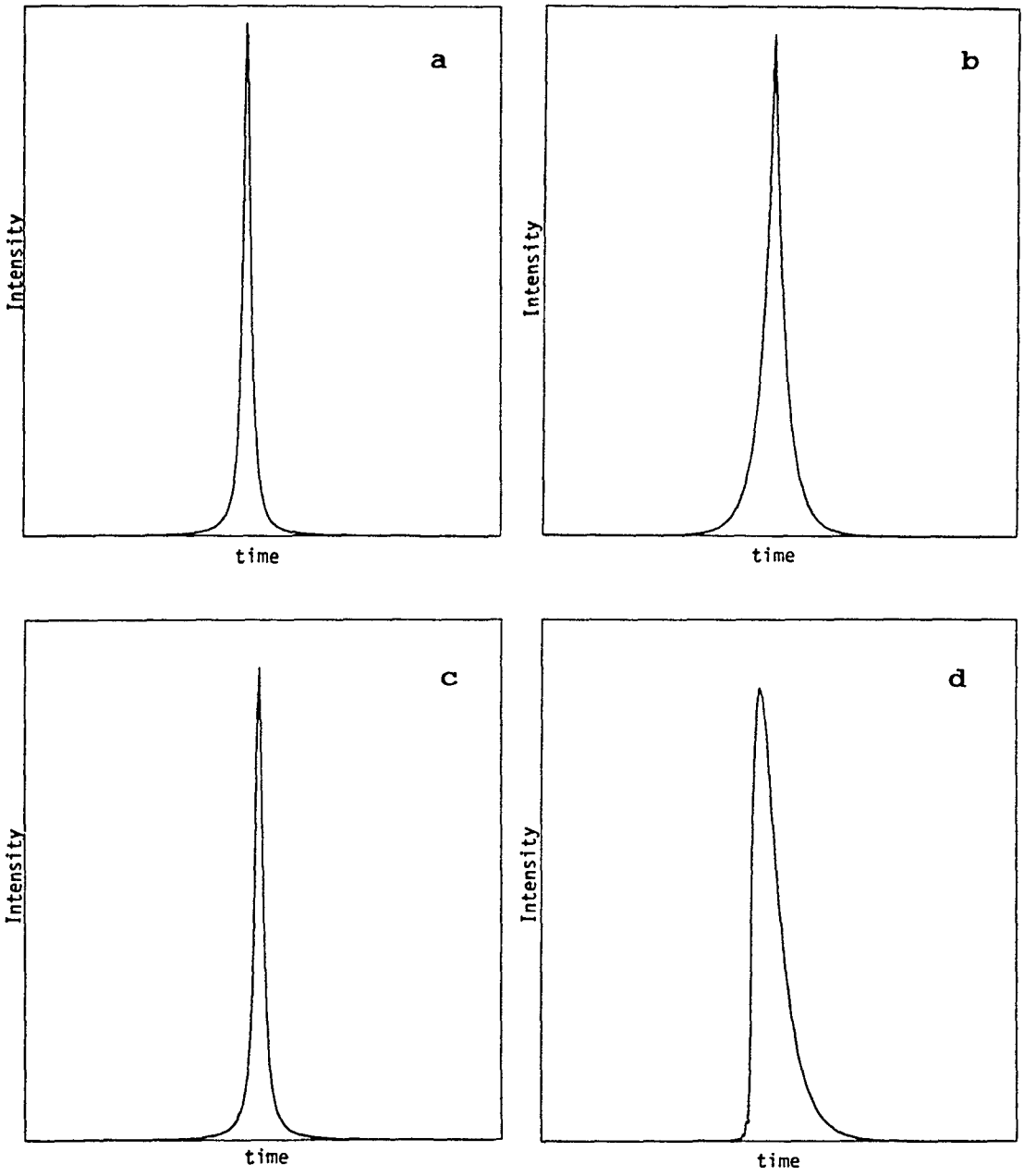

FIG. 4. Reconstructed waveforms. (a) and (b) are the results of the reconstruction of an autocorrelation of a Lorentzian (a) and a double-sided exponential (b). (c) and (d) show the results of the reconstruction of a triple correlation of a Lorentzian (c) and a double-sided exponential (d).

$i \leqslant j$. The differences between the results of these two approaches depend on whether the signal noise is signal dependent or independent. For signal-dependent noise, the two techniques produce identical results (reconstructed waveforms) because the noise is an integral part of the data. The averaging technique, on the other hand, reduces the effects of signal-independent noise on the reconstructed waveform.

III. RECONSTRUCTION SIMULATIONS

The following simulations will elucidate the properties of triple correlation. The resultant waveforms shown are from the reconstruction of a triple correlation or an autocorrelation. The simulations presented here are for "single-shot" experiments to more closely examine the effects of signal noise (both additive and multiplicative) on the resultant waveforms. The effects of time averaging will be considered later. A Lorentzian described by $1/[1 + [t/\tau]^2]$ and double-sided exponential described by $\exp(-t/\tau_1)$ $[1 - \exp(-t/\tau_2)]$ are used to illustrate the phase-preserving behavior of the triple correlation. Noise was added to the double-sided exponential (Fig. 3), and the subsequent reconstruction was compared to the deconvolution of an autocorrelation. The noise was generated from a pseudorandom number generator with a uniform distri-

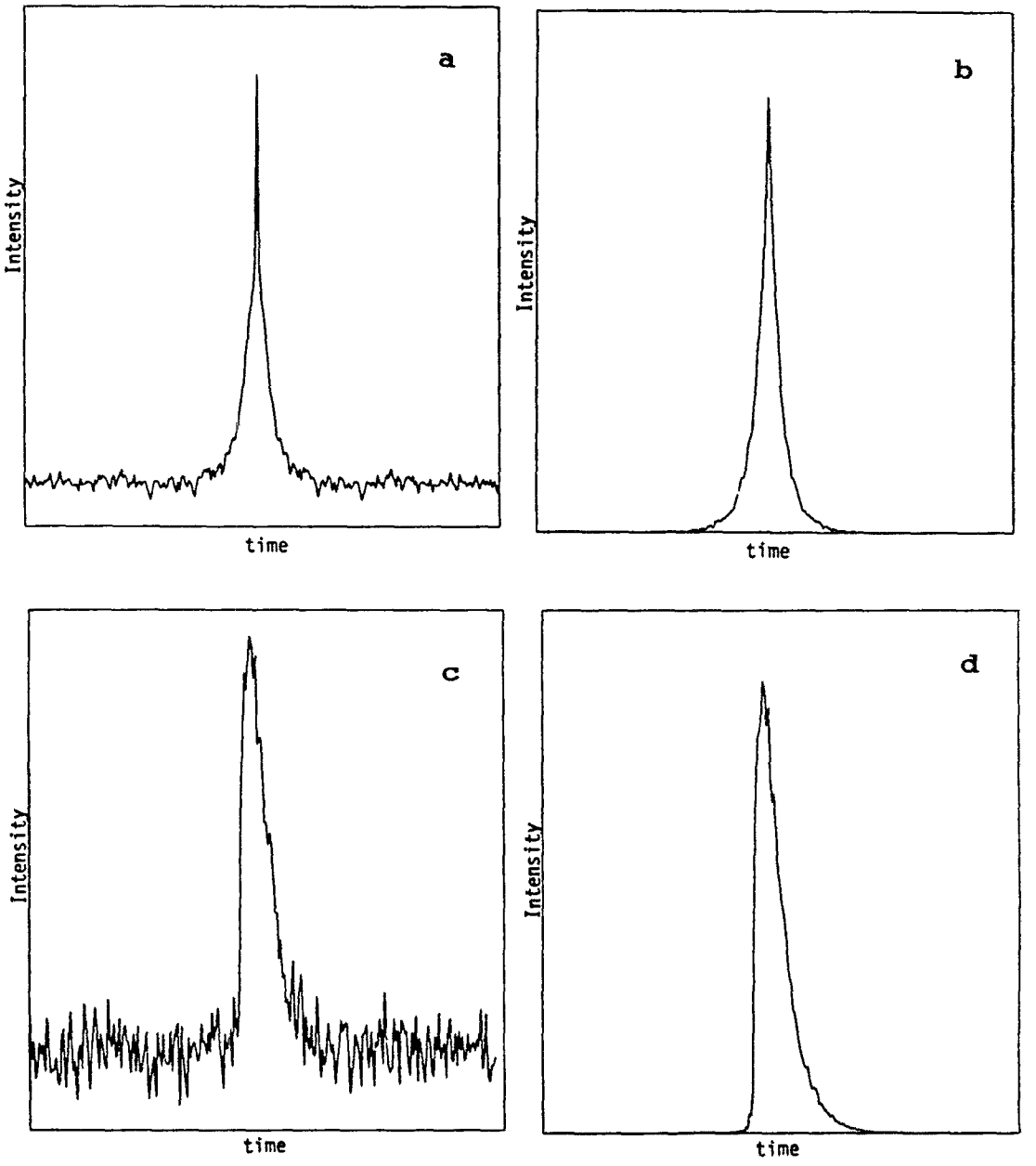

FIG. 5. Reconstruction of waveforms having a peak SNR of 5. (a) and (b) are the results of the reconstruction of an autocorrelation of the double-sided exponential with additive (a) and multiplicative (b) noise. (c) and (d) show the results of the reconstruction of a triple correlation of the double-sided exponential with additive (c) and multiplicative (d) noise.

bution and its randomness checked by autocorrelation. The waveform with additive noise is represented by

$$g(t)=f(t)+N'+cn(t), \tag{18}$$

and the waveform with multiplicative noise by

$$g(t)=f(t)[1+N'+cn(t)], \tag{19}$$

where c is a constant used to vary the signal-to-noise ratio, $n(t)$ is the zero-mean noise waveform, $f(t)$ is the double-sided exponential, and N' is the time-averaged value of $n(t)$. For the single-shot experiment N' is zero. For these simulations, c was set to 0.1 or 1, $n(t)$ varied from -1 to 1, and $f(t)$ ranged from 0 to 1. Figure 4 shows the reconstruction of the Lorentzian and double-sided exponential from an autocorrelation or triple correlation. Both techniques reproduce the original input Lorentzian successfully. The autocorrelation, however, has not been able to reproduce the exponential because of lost phase information, as exemplified by the symmetric result. On the other hand, the waveform reconstructed from the triple correlation has reproduced the exponential input accurately. The small oscillations in the reconstructed data will be discussed in the next section.

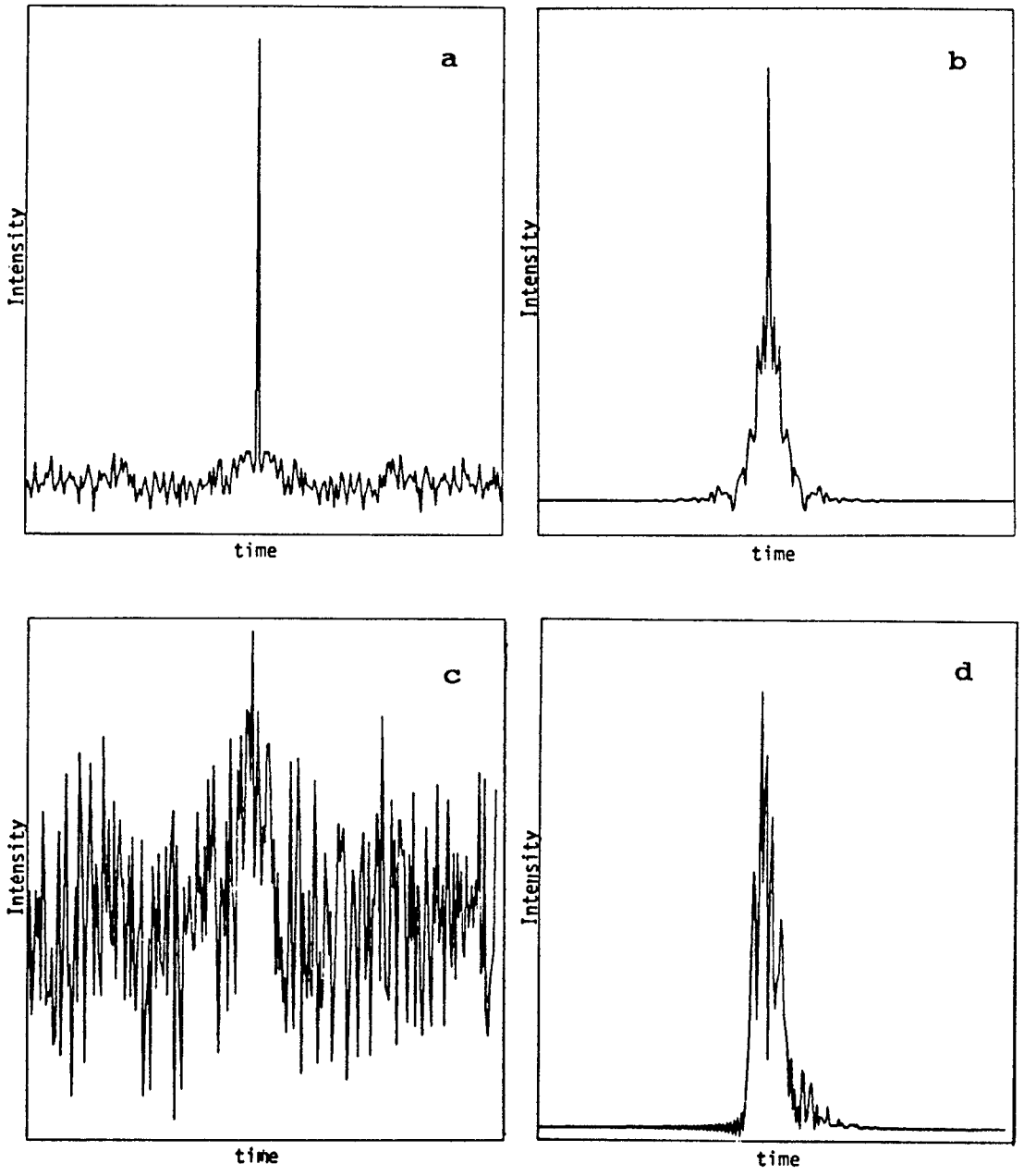

FIG. 6. Reconstruction of waveforms having a peak SNR of 0.5. (a) and (b) are the results of the reconstruction of an autocorrelation of the double-sided exponential with additive (a) and multiplicative (b) noise. (c) and (d) show the results of the reconstruction of a triple correlation of the double-sided exponential with additive (c) and multiplicative (d) noise.

A. Effects of non-time-averaged, signal-dependent noise

Figure 5 shows the reconstructed waveforms for inputs with 0.1-maximum-magnitude multiplicative or additive noise. Again, the autocorrelation has not been able to reproduce the original inputs, whereas the triple correlation provides accurate information. Figure 6 shows the reconstructed waveforms for input waveforms with 1.0-maximum-magnitude multiplicative and additive noise. These figures show that the triple correlation can reproduce the input waveforms accurately, with the exception of small added oscillations [compare Fig. 3(b) to Fig. 6(d)]. The origin of this noise will now be discussed.

Possible causes for the observed oscillations include phase error, machine error, or finite-record length error. Studies of the last two possibilities showed that they are not responsible for the observed oscillations. Therefore, the possibility of phase error was examined. The most likely candidate for this phase error is the assumption that loss of the first-harmonic phase was of no consequence. Therefore, the "lost" phase of the first harmonic will be considered in more detail. Recall (14) which describes the reconstruction of the first four harmonics. It can be seen that the phase angle of each harmonic is "off" by an integral multiple of the phase angle of the first harmonic, Φ_1. That is,

$$\Phi_i' = \Phi_i - i\Phi_1, \tag{20}$$

where Φ'_i is the phase angle of the reconstructed data, Φ_i is the phase angle of the original input signal, and i is the frequency index. At the folding (or Nyquist) frequency, the coefficient of the imaginary component is zero; consequently, the folding-frequency phase should also be zero. Therefore, any nonzero phase angle at the folding frequency is due to N times Φ_1. Therefore, we should be able to obtain the phase angle of the first harmonic by dividing the Nyquist-frequency phase by N. To test this, the Nyquist phase was obtained from a linearized phase function, divided by N to get the first-harmonic phase, and this phase component, multiplied by the index, was subtracted from the linear phase function. The results for the double-sided exponential with and without 1-maximum-magnitude multiplicative noise are shown in Fig. 7. The peak location is arbitrary. The important result is that the waveforms no longer manifest the oscillatory behavior. This implies that the oscillations were caused by a phase error and that this phase error is an errant multiple of Φ_1. Consequently, Φ_1 is important to correctly reconstruct the input pulse. Moreover, it appears the linear phase cannot be an arbitrary value. The constraints on the linear phase will now be explored.

A linear phase shift in the frequency domain and a time delay in the time domain are equivalent. The linear phase shift must be $\pm 2\pi/(N/k)$, where N/k is an integer and N is the length of the time record. N/k must be an integer because it represents a fraction of the time record, which can only be an integral multiple of the data's time interval (time between two successive points of the time record). Consequently, an erroneous linear phase becomes a sub-sampling error. For a linear phase shift of $\pm 2\pi/(N/k)$, the corresponding incremental phase shift for each frequency component is $\pm 2\pi j/(N/k)$ where j is the frequency index. The oscillations observed in the uncorrected-reconstructed signal were caused by a linear phase that did not fulfill the described prescription for proper linear phase.

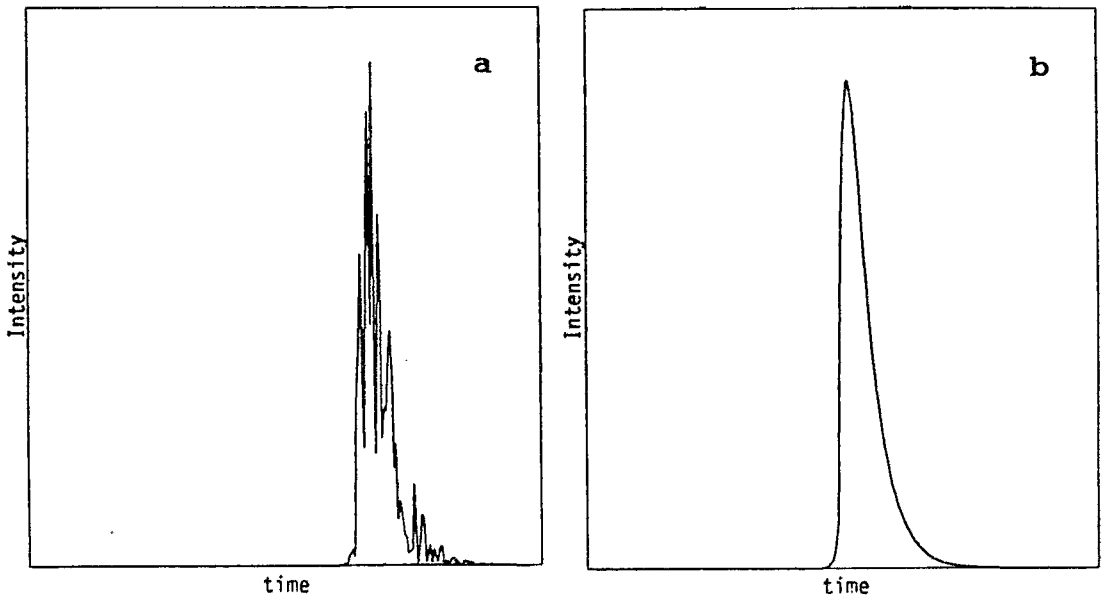

FIG. 7. Reconstructed waveforms with phase correction. Test waveform (a) with noise and (b) without multiplicative noise having a peak SNR of 0.5. Compare Figs. 3(b) (original input), 6(d) (reconstruction of Fig. 3(b) without phase correction), and 7(a) (reconstruction of Fig. 3(b) with phase correction). The profile of 7(a) accurately reproduces the profile of the 3(b).

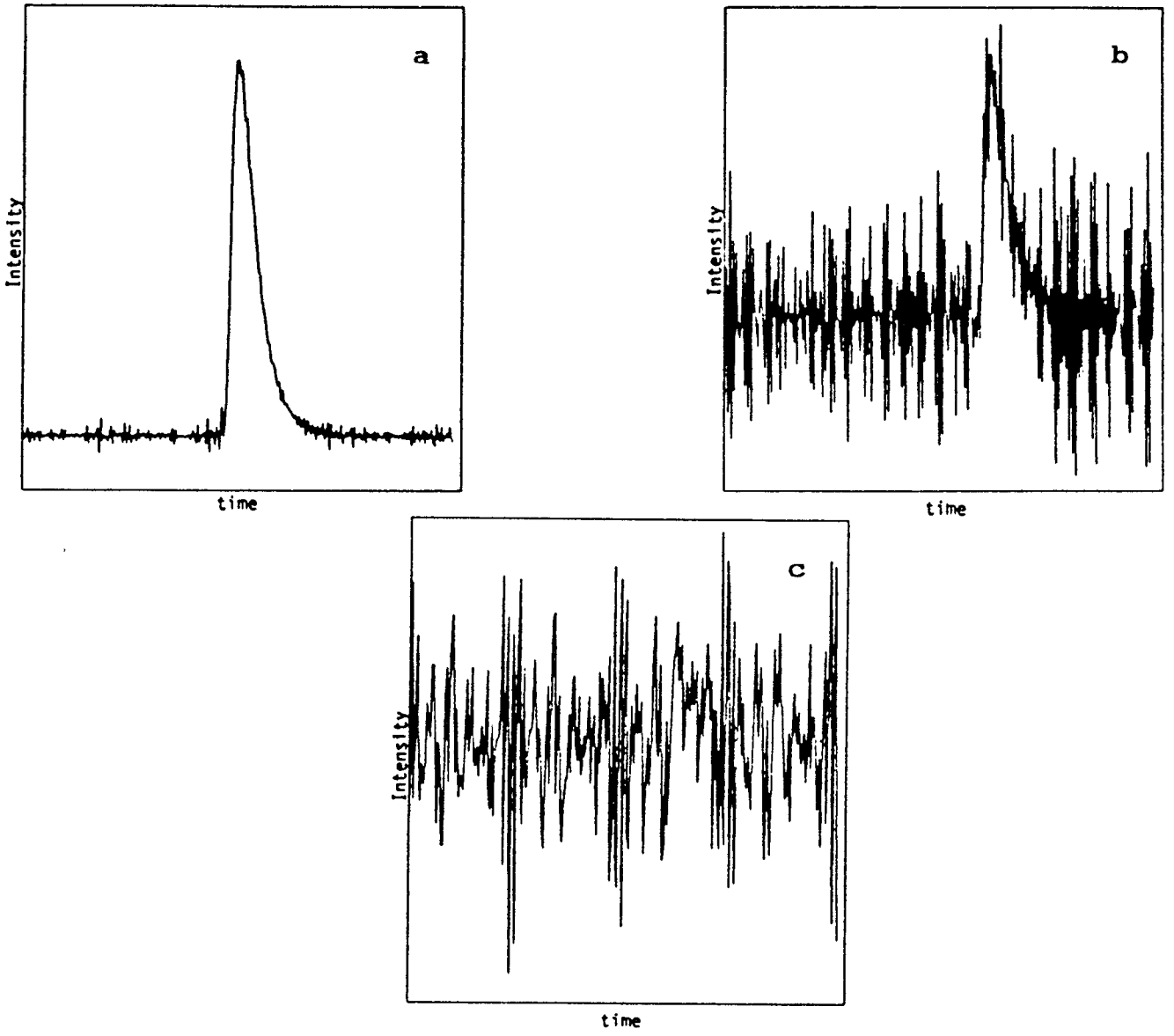

FIG. 8. Effects of signal-independent noise on waveform reconstruction without bispectrum averaging for (a) 10%, (b) 100%, and (c) 1000% noise-to-signal power.

B. Effects of non-time-averaged, signal-independent noise

Signal-independent noise is the noise added to the measured signal from an uncorrelated source, such as noise from the measurement electronics. For instance, if we are profiling repetitive pulses from a 100 MHz pulse train and the data acquisition rate is 1 kHz, then the signal at each data point has been sufficiently averaged so that the signal-dependent noise can be represented by its time-averaged value. On the other hand, each data point may have additional noise that it obtained from the measurement instruments (independent of the signal). So that is what we examine now, the effects of non-time-averaged, signal-independent noise. To this end, a triple correlation of a noise-free input (the double-sided exponential) and a noise plane, with a uniform distribution, were added. The noise plane was obtained by independently creating each column from a pseudo-random number generator. This insured that the noise was uniformly distributed across the data plane. The introduction of noise in this manner is not time averaged and is the worst-case scenario. The time-averaged case will simply add a constant background to the acquired data. Figure 8 shows the effect of the addition of signal-independent noise for noise-to-signal powers of 10%, 100%, and 1000%. This power ratio is the total power of the noise to that for the double-exponential in the 2-D window. Figure 9 shows the reconstructed data after using the averaging technique that was previously described. The recovered data have a dramatic improvement in the signal-to-noise ratio when the averaging reconstruction is used as compared to the non-averaged case. Consequently, the triple-correlation technique allows one to extract signals from very noisy backgrounds.

The relative level of signal-to-noise power can be im-

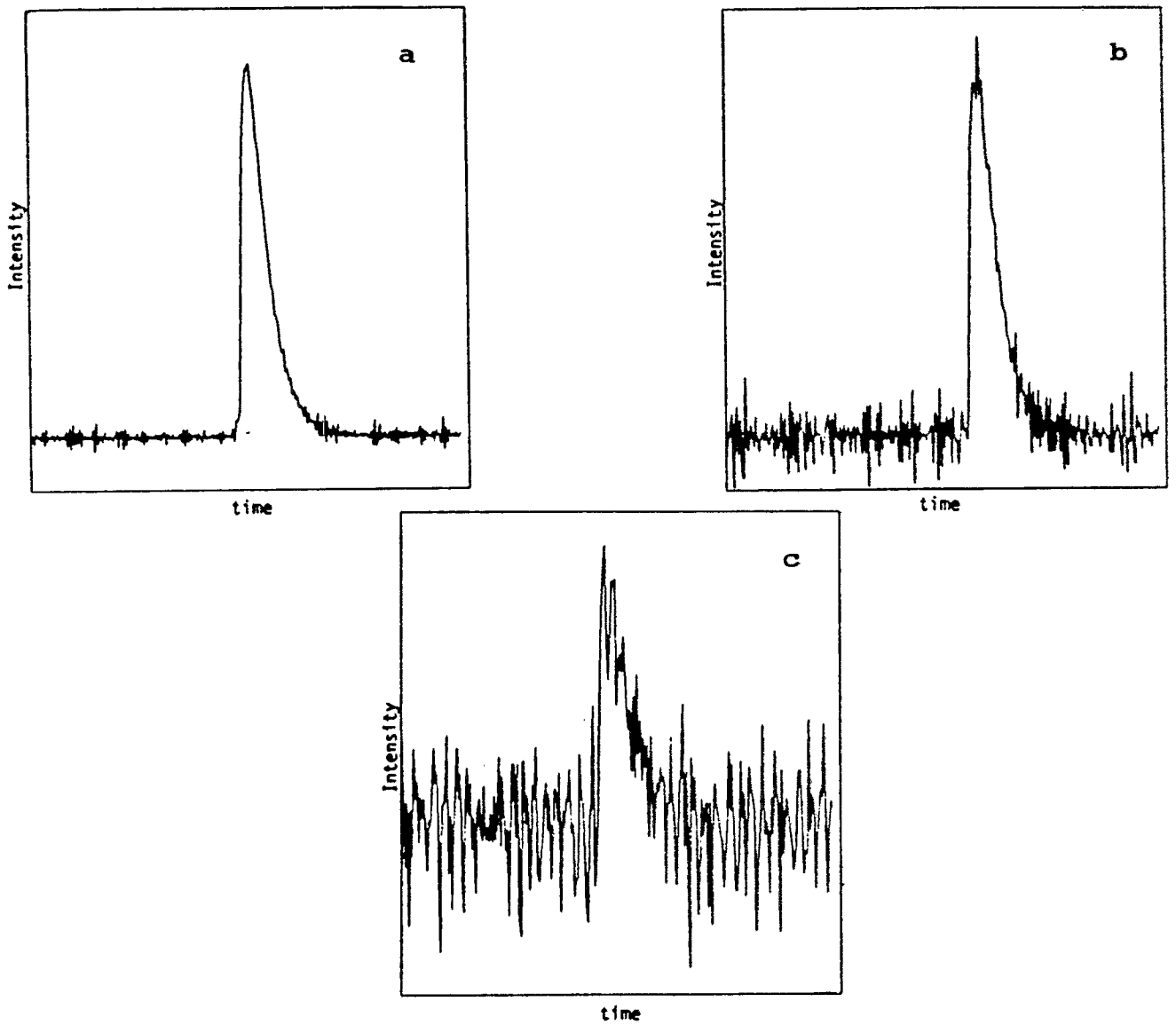

FIG. 9. Effects of signal-independent noise on waveform reconstruction with bispectrum averaging for (a) 10%, (b) 100%, and (c) 1000% noise-to-signal power.

proved by varying the time window, or equivalently, the time delays. Even though the peak signal-to-noise ratio does not change under this circumstance, the relative importance of the noise in the entire window decreases. To clarify, as the data plane is decreased, the average power of the signal is increased while the average power of the noise remains constant, thereby reducing the effects of noise on the reconstructed data.

IV. EFFECTS OF TIME-AVERAGED, SIGNAL-DEPENDENT NOISE

The effects of time-averaged noisy signals will be considered now. The operation of the triple correlator is such that each datum taken is the average of many occurrences, mimicking a boxcar-type averaging mode. Let the signals into the triple correlator be given by

$$I(t)=J(t)[1+M(t)]+A(t), \tag{21a}$$

$$I(t+\tau_1)=J(t+\tau_1)[1+M(t+\tau_1)]+A(t+\tau_1), \tag{21b}$$

$$I(t+\tau_2)=J(t+\tau_2)[1+M(t+\tau_2)]+A(t+\tau_2), \tag{21c}$$

where J is the noise-free signal, M is the multiplicative noise, and A is the additive noise. The time average of the noise terms is

$$\langle M(t)\rangle=\langle M(t+\tau_1)\rangle=\langle M(t+\tau_2)\rangle=M, \tag{22a}$$

$$\langle A(t)\rangle=\langle A(t+\tau_1)\rangle=\langle A(t+\tau_2)\rangle=A. \tag{22b}$$

The triple correlation of (21a), (21b), and (21c), and using (22a) and (22b) for the time-average value for the noise, is

$$\int I(t)I(t+\tau_1)I(t+\tau_2)dt = A^3 + A^2(4M+2)\int J(t)dt + A(M^2+2M+1)\int J(t)J(t+\tau_1)dt$$
$$+ A(M^2+2M+1)\int J(t)J(t+\tau_2)dt + A(M^2+2M+1)\int J(t+\tau_1)J(t+\tau_2)dt$$
$$+ (M^3+3M^2+3M+1)\int J(t)J(t+\tau_1)J(t+\tau_2)dt. \quad (23)$$

The first five terms to the right of the equal sign in (23) are noise terms. Each noise term can be obtained from the data plane (see Fig. 10) and subsequently removed from the data. To understand this, assume the delays have been adjusted so that zero delay is centered in the data plane and that the delays are sufficiently long so that all noise contributions can be measured. The first noise term can be obtained from any region of the data plane where the three pulses from each of the three beams have not interacted, that is, in regions where only the noise is interacting. The second noise term will also be distributed uniformly across the data plane, and can be obtained from the data in areas where one pulse is interacting with the noise of the other two beams. The time average of the multiplicative noise, M, may be obtained by comparing the power of the second noise term to that from a power meter. For example, assume the measurement electronics are well characterized, A has been measured, and the integral of $J(t)$ is simply the average power; then the slope of a plot of power-meter output versus second-noise-term power will give M. The next three noise terms are autocorrelation terms and may be obtained from regions of the data plane where the pulses from two of the beams have interacted with each other and with noise of the third beam. Consequently, one can remove the effects of time-averaged, signal-dependent additive and multiplicative noise from the data plane.

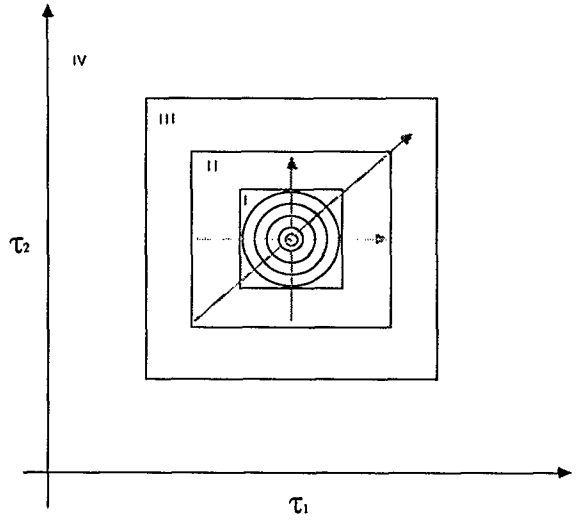

FIG. 10. Projection of data on $\tau_1 - \tau_2$ plane to emphasize the effects of noise on the data [see Eq. (23)]. The cube of the time-averaged value of the additive noise is contained in the entire data plane, but it is the only noise contribution in region IV. The triple-correlation noise term caused by the correlation of noise from two beams and a pulse from the third is found in regions I, II, and III. The autocorrelation-noise terms (three) are caused by the correlation of noise from one beam and pulses from the other two beams and their effects are found in regions I and II. The result of the triple correlation of pulses from all three beams is found only in region I. The circles represent a contour plot of a noise-free, triply correlated, symmetric pulse. The dashed arrows represent the three autocorrelation-noise contributions and how they add to the data plane.

V. DISCUSSION

The technique proposed here for the measurement of the full temporal intensity profile of ultrashort (picosecond and femtosecond duration) laser pulses is based on recording the triply correlated intensity of the pulses. This technique uses two consecutive nonlinear optical interactions and three replicas of the same laser input to produce ameasurable signal that has the same optical frequency content as the input pulse. Because the output signal has the same frequency content as the input, this technique does not require complex third-harmonic-generation measurement. In this respect, this proposed method is different from any other previously reported techniques. The temporal resolution of this technique is dependent on the inherent response times of available nonlinear materials used and on the spatial resolution of the time delay stages. With piezoelectric crystals, almost infinite resolution for the time delays can be achieved. Therefore, the temporal resolution of this triple correlator will be limited ultimately by the speed of the nonlinear optical materials, and is expected to give 1 fs or less resolution.

ACKNOWLEDGMENTS

We would like to thank Richard G. Geyer, Douglas, L. Franzen, Mark T. Ma, and Matt Young for their comments on this paper. We would also like to thank William A. Kissick and William L. Gans for administrative support.

[1] G. A. Mourou, D. M. Bloom, and C.-H. Lee, eds. *Picosecond Electronics and Optoelectronics, Proceedings of the Topical Meeting*, Lake Tahoe, NV, March 1985 (Springer, New York, 1985).
[2] F. J. Leonberger, C.-H. Lee, F. Capasso, and H. Markoc, Eds., *Picosecond Electronics and Optoelectronics, II, Proceedings of the Second OSA-IEEE*, Incline Village, NV, January 1987 (Springer, New York, 1987).
[3] D. H. Auston and K. B. Eisenthal, *Ultrafast Phenomena IV, Proceedings of the Fourth International Conference*, Monterey, CA, June 1984 (Springer, New York, 1984).

[4] G. R. Fleming and A. E. Siegman, *Ultrafast Phenomena V, Proceedings of the Fifth OSA Topical Meeting,* Snowmass, CO, June 1986 (Springer, New York, 1986).
[5] C. H. Lee, *Picosecond Optoelectronic Devices* (Academic, New York, 1984).
[6] R. Jain, Ed., *Characterization of Very High Speed Semiconductor Devices and Integrated Circuitry,* SPIE (International Society for Optical Engineering, Bellingham, WA, 1987), Vol. 795.
[7] W. Sibbett, "Synchroscan streak camera system," *High Speed Photography and Photonics,* Proc. SPIE (International Society for Optical Engineering, Bellingham, WA, 1982), Vol. 348.
[8] A. Yariv and D. M. Pepper, Opt. Lett. **1**, 16 (1977).
[9] T. R. O'Meara and A. Yariv, Opt. Eng. **21**, 237 (1982).
[10] J. Janszky, G. Corradi, and D. S. Hamilton, Appl. Opt. **23**, 8 (1984).
[11] J. Buchert, R. Dorsinville, P. Delfyett, S. Krimchansky, and R. R. Alfano, Opt. Commun. **52**, 433 (1985).
[12] J. Janszky and G. Corradi, Opt. Commun. **60**, 251 (1986).
[13] N. Bloembergen, *Nonlinear Optics, A Lecture Note and Reprint Volume,* (Benjamin, New York, 1965).
[14] Y. R. Shen, *The Principles of Nonlinear Optics* (Wiley, New York, 1984).
[15] R. L. Fork and F. A. Beisser, Appl. Opt. **17**, 3534 (1978).
[16] J. P. Curtis and J. E. Carroll, Int. J. Electron. **60**, 87 (1986).
[17] E. W. Van Stryland, Opt. Commun. **31**, 93 (1979).
[18] K. L. Sala, G. A. Kenney-Wallace, and G. E. Hall, IEEE J. Quantum. Electron. **QE-16**, 990 (1980).
[19] J.-C.M. Diels, J. J. Fontaine, I. C. McMichael, and F. Simoni, Appl. Opt. **24**, 1270 (1985).
[20] B. H. Kolner and M. Nazarathy, Opt. Lett. **14**, 630 (1989).
[21] J. E. Rothenberg and D. Grischkowsky, Opt. Lett. **12**, 99 (1987).
[22] H. Gamo, J. Appl. Phys. **34**, 875 (1963).
[23] B. Wirnitzer, Opt. Commun. **48**, 225 (1983).
[24] H. Bartlet, A. W. Lohmann, and B. Wirnitzer, Appl. Opt. **23**, 3121 (1984).